



Swansea University
Prifysgol Abertawe



Cronfa - Swansea University Open Access Repository

This is an author produced version of a paper published in:

Nanoscale

Cronfa URL for this paper:

<http://cronfa.swan.ac.uk/Record/cronfa37598>

Paper:

Van Keulen, G. (in press). Organic matter identifies the nano-mechanical properties of native soil aggregates.

Nanoscale

<http://dx.doi.org/10.1039/C7NR07070E>

This item is brought to you by Swansea University. Any person downloading material is agreeing to abide by the terms of the repository licence. Copies of full text items may be used or reproduced in any format or medium, without prior permission for personal research or study, educational or non-commercial purposes only. The copyright for any work remains with the original author unless otherwise specified. The full-text must not be sold in any format or medium without the formal permission of the copyright holder.

Permission for multiple reproductions should be obtained from the original author.

Authors are personally responsible for adhering to copyright and publisher restrictions when uploading content to the repository.

<http://www.swansea.ac.uk/library/researchsupport/ris-support/>

Organic matter identifies the nano-mechanical properties of native soil aggregates

S.A.Gazze^{a*}, I.Hallin^b, G.Quinn^a, E.Dudley^a, P.G.Matthews^b, P.Rees^c, G.van Keulen^{a#}, S.H.Doerr^d, L.W.Francis^{a~}

Salvatore A. Gazze^{a*}, Ingrid Hallin^b, Gerry Quinn^c, Ed Dudley^a, G. Peter Matthews^b, Paul Rees^d, Geertje van Keulen G.^a, Stefan H. Doerr^e, Lewis W. Francis.^a

^a Swansea University Medical School , Singleton Campus, Swansea SA2 8PP, UK

^b Faculty of Science and Engineering, Plymouth University, Drake Circus, Plymouth PL4 8AA, UK

^c Ruđer Bošković Institute, Bijenička cesta 54, 10000, Zagreb, Croatia

^d College of Engineering, Swansea University, Bay Campus, Swansea, SA1 8EN, UK

^e Department of Geography, College of Science, Swansea University, Singleton Campus, Swansea SA2 8PP, UK

*e-mail: s.a.gazze@swansea.ac.uk;

Cite this: DOI: 10.1039/c7nr07070e

Received 21st September 2017,

Accepted 28th November 2017

First published online on 14 Dec 2017

rsc.li/nanoscale

Abstract

Localized variations at the nanoscale in soil aggregates and in the spatial organisation of soil organic matter (SOM) are critical to understanding the factors involved in soil composition and turnover. However soil nanoscience has been hampered by the lack of suitable methods to determine soil biophysical properties at nanometre spatial resolution with minimal sample preparation. Here we introduce for the first time an Atomic Force Microscopy (AFM)-based Quantitative Nano-Mechanical mapping (QNM) approach that allows the characterisation of the role of SOM in controlling surface nano-mechanical properties of soil aggregates. SOM coverage resulted in an increased roughness and surface variability of soil, as well as in decreased stiffness and adhesive properties. The latter also correlates with nano- to macro- wettability features as determined by contact angle measurements and Water Drop Penetration Time (WDPT) testing. AFM thus represents an ideal quantitative tool to complement existing techniques within the emerging field of soil nanoscience.

Several important biogeochemical reactions occur in soil at the nanoscale and potentially affect soil functioning at the field-scale^{1–5}: nanoscale molecular interactions in soil microaggregates are believed to play an important role for the distribution and long-term preservation of soil carbon and nutrients^{1,5}; nutrient root exudation takes place in micron-scale level interfaces with minerals and microbial fauna⁴, while microbial reactions, which also affect pollutants and SOM storage through mineralization, take place in microaggregate crevices⁶. Soil nanoscience has been pioneered by advanced microscopic and spectrometric techniques such as secondary ion mass spectroscopy (NanoSIMS) and X-ray spectromicroscopy, which are increasingly being applied to soil studies and for the characterisation of SOM at both the micro and nano scale^{2,7–10}. Suitable methods for nanoscale biophysical characterization of soil have been less explored. A promising approach is represented by Atomic Force Microscopy (AFM)¹¹, a nanoscale topographical and nanomechanical contact probe microscope that has so far been preferentially applied to inspect relatively flat samples such as single biomolecules deposited onto atomically flat substrates (*e.g.* mica, graphite, SiO₂)¹². Recent technological advances, centred on enhanced feedback electronics and new scanning modes, now allow significantly better accuracy in probe-surface tracking, enabling novel AFM characterisation of more heterogeneous samples^{13,14} and, as a result, AFM is becoming increasingly applied in soil studies^{15–18}.

In the present work, a standardized approach to analyzing soil aggregate topography with high spatial resolution nano-mechanical mapping is developed using AFM. The combination of AFM imaging and probe selection has been first optimised: probes with short tips (such as probes 1 and 2 in Fig. S1A) produced image artefacts in the form of parallel terraces, as a result of the cantilever beam touching the soil surface (Fig. S1B and C). Cantilevers having longer tips (such as probes 4 and 5 in Fig. S1A) were less prone to surface contact by the main cantilever beam, resulting in a more efficient soil surface tracking (Fig. S1C). Probes were also selected based on their spring constant values: very low values negatively affect the surface tracking performance, while too high values decrease the nanomechanical sensitivity, such as measurements of adhesive properties for both mineral and SOM components. Finally, Bruker's proprietary Peak Force Tapping (PFT)¹⁹ enabled greater force control, tracking the irregular soil surface more consistently than traditional Tapping Mode (Fig. S2). In PFT-AFM the cantilever oscillates in a sinusoidal mode over the sample surfaces at low frequencies (between 0.25-2 Hz), which allows for a better surface tracking of rough samples, coupled with a precise control of the force applied during scanning.

Reproducible AFM imaging of soil nanoscale surfaces complements more traditional Scanning Electron Microscopy (SEM) micrographs, revealing almost identical microscale topographical features (Fig. 1A and B) on soil aggregates derived from a common soil type (silt loam from acid sedimentary rock, Cefn Bryn, Wales), which was previously characterized using standard analyses (Table S1). The AFM approach developed here is shown from Fig. 1C to F, where an initial scan area of 100 μm^2 (Fig. 1C) is reduced progressively to focus on single soil particles (Fig. 1D) and nanometre-sized areas (Fig. 1E and F). Areas of the aggregates occupied by SOM were identifiable, with rougher surface topography than the underlying flat mineral surfaces, Fig. 1E, thus enabling the distribution of SOM to be estimated with unparalleled spatial resolution.

The QNM mode supplements PFT scanning, in QNM-PFT, with fully quantitative pixel-by-pixel nano-mechanical mapping, resolving several surface properties such as InPhase, Fig. 1F. The latter is comparable to the Phase signal in traditional Tapping Mode and, as such, identifies the presence of differences in material properties²⁰. Adopting the presentation of complimentary AFM outputs allows the identification of previously unrecognisable soil nanoscale components and contaminants, resolving the presentation of aggregate SOM coverage at higher resolution than the topographical image, as revealed in Fig. 1E and F, by comparing the topographical and InPhase outputs for the same scanned area.

Both the biotic and abiotic components of soil aggregates were imaged using PFT-QNM before (control sample: CON) and after an acid-peroxide wash (APW sample), which removes most of the organic matter content and hence allows to investigate the role of SOM spatial distribution in defining soil properties (Fig. 2). While topographic maps reveal irregular soil aggregate surfaces in the presence and absence of SOM (Fig. 2A,C,E,G), the presence of organic matter is often more easily identified when the other signals are considered, alone or in combination. For example, the elastic modulus map of a CON area, calculated using the Derjaguin–Muller–Toporov (DMT) model²¹, reveals two distinct regions (Fig. 2B), not easily visible in the respective topography map (Fig. 2A). The upper area has a median elastic modulus E of about 7.6 GPa, while the lower area has a two-fold decrease in E (3.1 GPa) due to the higher amount of SOM that reduces the local stiffness. Indeed, the stiffer upper region has an E value close to an area of APW soil (8.7 GPa, Fig. 2F), where the mineral phase is the only contributor to the local stiffness. In another CON area the topography image reveals a planar surface occupied by few rounded components (Fig. 2C) whose presence is unveiled more clearly in the adhesion output, Fig. 2D, together with filamentous SOM structures not visible in the topographical map. AFM adhesion is measured as the force needed to detach the cantilever tip from the soil surface.

SOM components presents lower adhesion values compared to the underlying mineral surface, Fig. 2D; In contrast, the adhesion map for APW soil in Fig. 2H reveals the presence of one main contribution, further validating the role of organic matter in affecting local surface properties.

The potential of the nanoscale AFM approach is further shown in Fig. 3, which plots the data extracted from 30 areas, using the same approach discussed in Fig. 1C-F and on the same number of soil aggregates across the two sample types (CON and APW). Consistent with what has been shown in this work, organic matter had a considerable influence on several nanoscale properties, with a decrease in adhesion and stiffness and an increase in roughness and heterogeneity, the latter revealed by InPhase data. Indeed, InPhase for APW soil, Fig. 3A, presents a narrower range than CON soil, suggesting lower surface variability due to SOM removal and the subsequent prevalence of the only

mineral constituent. In CON soil we observed a general decrease in surface stiffness, Fig. 3B, with the median DMT stiffness about two times lower than that for APW soil (3.81 ± 0.03 GPa and 9.05 ± 0.03 GPa, respectively) due to the larger amount of organic matter on CON soil. The latter has a wider spread with two overlapping distributions, D1 and D2 in Fig. 3B, where distribution D2 presents a higher incidence of organic phase compared to distribution D1: this explains the narrow shift of D2 towards lower stiffness values. Single SOM areas range in stiffness from 290 MPa to about 1 GPa; while these values belong to the stiffness range of biomolecules as calculated using AFM²², the values at the higher spectrum end could be partly determined by the dry or dehydrated SOM components. A state which may produce an increased surface stiffness, decreasing the fold difference relative to the bare mineral surface itself.

SOM presence is expected to affect surface nano-roughness as well, as already mentioned for Fig. 1C. Roughness R_q calculated from the 3D images showed that sample CON was significantly rougher (t-test p value < 0.001) than sample APW, with R_q values of 12.7 ± 1.2 nm and 5.2 ± 0.5 nm, respectively (Fig. 3C). This is consistent with what has been already observed for mineral particles from soils and groundwater-exposed minerals^{23–25}. For example, Cheng et al. (2008)²⁵ observed an increased sample roughness for humic acid deposited on acid-washed quartz sand, although an opposite trend was observed for mineral quartz particles from soil with increasing organic matter content. SOM has also been previously reported to collect in the rougher areas of soil particle surfaces⁸, thus further increasing local roughness, which in turn has an effect on soil wettability through the Cassie-Baxter effect²³.

When compared to other micro-to- macroscale properties such as bulk SOM amount and wettability properties, comprehensive multiscale soil profiles can be identified, as summarised in Table 1 for both CON and APW soils. Surface occupancy of organic matter on soil CON different areas, measured as shown in Fig. 1F for a single area, ranges from almost 0 to 100%, with an average value of $50\% \pm 7\%$. As expected, APW soil samples have lower SOM surface coverage, $8\% \pm 2\%$, which in part may represent non-extractable organic residues²⁶. Soil organic matter content determined on bulk soil, with a value of $5.60 \pm 0.02\%$ (Table S1), gives no indication of both the fraction of mineral surfaces covered in organic matter and of the high variability in surface coverage, as reported through AFM. This attests the need to focus on the nanoscale for an accurate description of SOM spatial distribution and properties, as already pointed out by Lehmann et al. (2008)¹ using X-ray spectromicroscopy.

AFM adhesion data, which shows higher values for APW compared to CON samples (Fig. 3D), has been previously used to assess hydrophilicity states of several substrates with both silicon and silicon nitride tips^{25,27,28}: sample hydrophilicity is expected to be associated with evident AFM pull-off adhesion values due to the formation of a water meniscus between the cantilever tip and the sample surface²⁹, as schematically shown in Fig. S3A. Measurements in water determines a considerable decrease in this pull-off force as the meniscus force disappears, as reported in Kim et al. (2008)²⁷, as well shown herein for a subset of CON soil areas (Fig. S3B). In the present study soil wettability has been experimentally quantified through different approaches and at increasing scales using AFM adhesion maps, Fig. 3D and Table 1, nano- and microgoniometry, and Water Drop Penetration Tests (WDPT), Table 1. All these techniques found higher water repellence in CON samples compared to acid-washed APW samples, supporting the widely accepted notion that the presence of SOM is the principle agent for reducing the hydrophilicity of soil mineral components^{30,31}.

Conclusions

In the present work, quantitative AFM was optimized to enable a routine *ex-situ* analysis of intact soil aggregates under ambient conditions. Using this approach, we showed that AFM can now be used to obtain nanoscale morphological and mechanical profiling of soil components at nanoscale resolution. The advancement of soil nanoscience and the need to examine events taking place at the nanoscale will undoubtedly benefit from AFM as the sole available technique to probe the real 3D structure and several mechanical properties of soil at this resolution. A particularly notable finding from this study is that these nanomechanical properties can be directly linked to SOM % coverage values, identifying and quantifying the role of SOM in determining several nanoscale properties such as surface roughness and stiffness. Moreover, it has been possible to link nanoscale and macroscale wettability, thus providing direct evidence for the role of SOM in affecting bulk soil wettability. Future applications of this new approach include, but are not limited to, the prospect of (a) following in *real-time* and *ex-situ* specific biogeochemical reactions occurring in soil and, (b) better understanding how biology can affect soil mechanical characteristics at different length scales.

Acknowledgements

This work was supported by the Natural Environment Research Council (grant n. NE/K004638/1 and NE/K004212/1).

Conflicts of interest

The authors declare that there is no conflict of interests regarding the publication of this paper.

Notes and references

- 1 J. Lehmann, D. Solomon, J. Kinyangi, L. Dathe, S. Wirick and C. Jacobsen, *Nat. Geosci.*, 2008, **1**, 238–242.
- 2 D. Solomon, J. Lehmann, J. Harden, J. Wang, J. Kinyangi, K. Heymann, C. Karunakaran, Y. Lu, S. Wirick and C. Jacobsen, *Chem. Geol.*, 2012, **329**, 53–73.
- 3 I. M. Young, J. W. Crawford, N. Nunan, W. Otten and A. Spiers, in *Advances in Agronomy*, Elsevier Inc., 1st edn., 2008, vol. 100, pp. 81–121.
- 4 J. M. Norton and M. K. Firestone, *Soil Biol. Biochem.*, 1996, **28**, 351–362.
- 5 M. W. I. Schmidt, M. S. Torn, S. Abiven, T. Dittmar, G. Guggenberger, I. A. Janssens, M. Kleber, I. Kögel-Knabner, J. Lehmann, D. A. C. Manning, P. Nannipieri, D. P. Rasse, S. Weiner and S. E. Trumbore, *Nature*, 2011, **478**, 49–56.
- 6 N. Nunan, I. M. Young, J. W. Crawford and K. Ritz, in *The Spatial Distribution of Microbes in the Environment*, eds. R. B. Franklin and A. L. Mills, Springer Netherlands, Dordrecht, 2007, pp. 61–85.
- 7 M. Keiluweit, J. J. Bougoure, L. H. Zeglin, D. D. Myrold, P. K. Weber, J. Pett-Ridge, M. Kleber and P. S. Nico, *Geochim. Cosmochim. Acta*, 2012, **95**, 213–226.
- 8 C. Vogel, C. W. Mueller, C. Höschen, F. Buegger, K. Heister, S. Schulz, M. Schlöter and I. Kögel-Knabner, *Nat. Commun.*, 2014, **5**, 1–7.

- 9 P.-J. Hatton, L. Remusat, B. Zeller and D. Derrien, *Rapid Commun. Mass Spectrom.*, 2012, **26**, 1363–1371.
- 10 L. Remusat, P. J. Hatton, P. S. Nico, B. Zeller, M. Kleber and D. Derrien, *Environ. Sci. Technol.*, 2012, **46**, 3943–3949.
- 11 G. Binnig, C. F. Quate and C. Gerber, *Phys. Rev. Lett.*, 1986, **56**, 930–933.
- 12 A. Ikai, *Surf. Sci. Rep.*, 1996, **26**, 261–332.
- 13 E. Behazin, E. Ogunsona, A. Rodriguez-Urbe, A. K. Mohanty, M. Misra and A. O. Anyia, *BioResources*, 2016, **11**, 1334–1348.
- 14 I. M. Khan, L. Francis, P. S. Theobald, S. Perni, R. D. Young, P. Prokopovich, R. S. Conlan and C. W. Archer, *Biomaterials*, 2013, **34**, 1478–1487.
- 15 S. Cheng, S. H. Doerr, R. Bryant and C. J. Wright, *Soil Sci. Soc. Am. J.*, 2010, **74**, 1541–1552.
- 16 P. A. Gerin and Y. F. Dufrene, *Colloids Surfaces B Biointerfaces*, 2003, **28**, 295–305.
- 17 G. E. Schaumann and Y. K. Mouvenchery, *J. Soils Sediments*, 2012, **12**, 48–62.
- 18 Y. K. Mouvenchery, A. Miltner, C. Schurig, M. Kästner and G. E. Schaumann, *J. Plant Nutr. Soil Sci.*, 2016, **179**, 48–59.
- 19 Bruker, *Peak Force QNM User Guide*, 2011.
- 20 I. Schmitz, M. Schreiner, G. Friedbacher and M. Grasserbauer, *Appl. Surf. Sci.*, 1997, **115**, 190–198.
- 21 B. Derjaguin, V. Muller and Y. Toporov, *J. Colloid Interface Sci.*, 1975, **53**, 314–326.
- 22 N. E. Kurland, Z. Drira and V. K. Yadavalli, *Micron*, 2012, **43**, 116–128.
- 23 V. K. Truong, E. A. Owuor, P. Murugaraj, R. J. Crawford and D. E. Mainwaring, *J. Colloid Interface Sci.*, 2015, **460**, 61–70.
- 24 C. Gaebel, J. R. Lead, J. C. Renshaw and J. H. Tellam, *J. Contam. Hydrol.*, 2009, **108**, 46–53.
- 25 S. Cheng, R. Bryant, S. H. Doerr and P. Rhodri Williams, *J. Microsc.*, 2008, **231**, 384–394.
- 26 P. Burauel and F. Führ, *Environ. Pollut.*, 2000, **108**, 45–52.
- 27 D. I. Kim, J. Grobelny, N. Pradeep and R. F. Cook, *Langmuir*, 2008, **24**, 1873–1877.
- 28 J. Colson, L. Andorfer, T. E. Nypelö, B. Lütke-meier, F. Stöckel and J. Konnerth, *Colloids Surfaces A Physicochem. Eng. Asp.*, 2017, **529**, 363–372.
- 29 R. Jones, H. M. Pollock, J. A. S. Cleaver and C. S. Hodges, *Langmuir*, 2002, **18**, 8045–8055.
- 30 S. H. Doerr, R. A. Shakesby and R. P. D. Walsh, *Earth Sci. Rev.*, 2000, **51**, 33–65.
- 31 M. Ma'shum, M. E. Tate, G. P. Jones and J. M. Oades, *J. Soil Sci.*, 1988, **39**, 99–110.

Figures and Tables

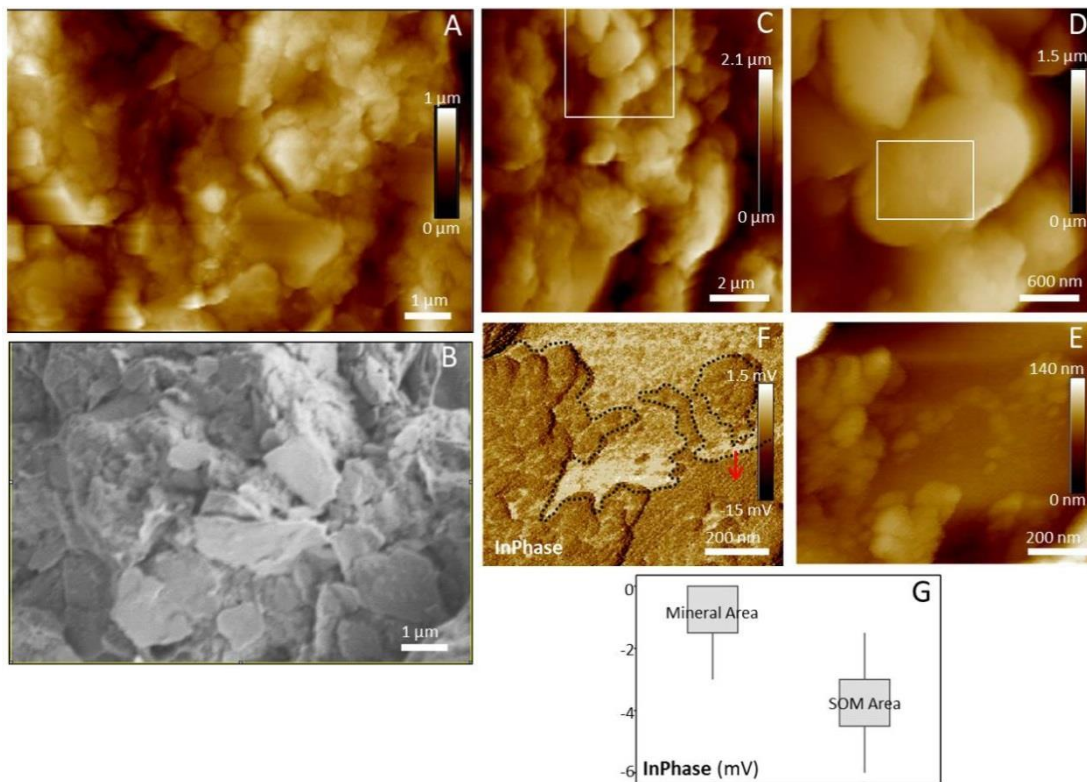


Figure 1. Visualization of soil aggregates with QNM-AFM. A) Imaged in PF-QNM mode. B) SEM soil image. C) Topography of a 100 µm² area. The box indicates the region represented in D). E) High-resolution topography of the area indicated by the box in D). F) InPhase output of the area shown in E. Darker areas indicate the presence of organic matter, which occupies 61 % of the imaged area, calculated using ImageJ. The red arrow indicates an area where SOM is visible using InPhase, but not using topography in E. G) Boxplot graph of the InPhase values for SOM and bare mineral areas. Median values are -1.5 mV and -4.5 mV for mineral areas and SOM areas, respectively.

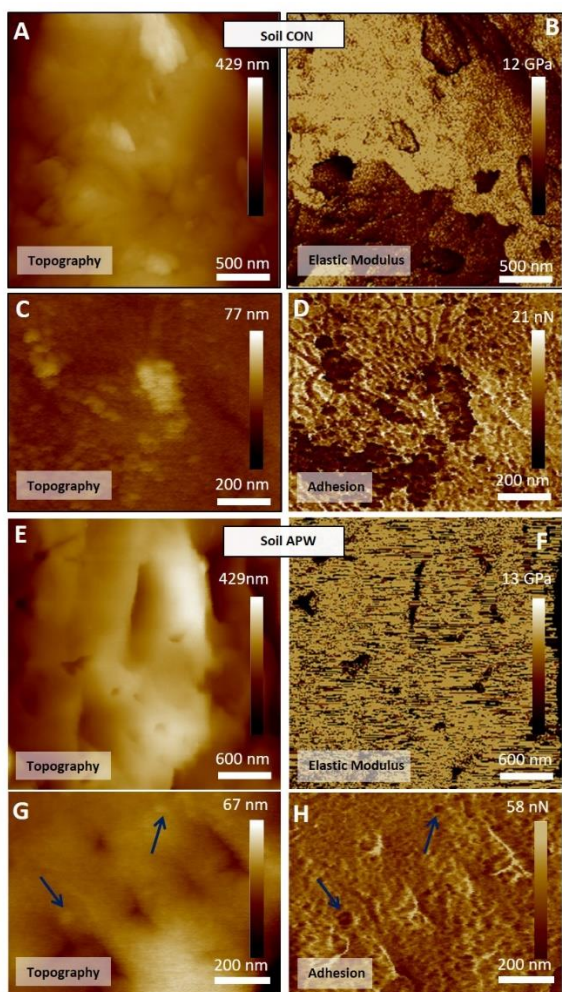


Figure 2. **QNM outputs of CON and APW soil.** A) Topography of a $6.7 \mu\text{m}^2$ area of CON soil, with Elastic Modulus E map shown in B. Modulus is calculated according to the Derjaguin–Muller–Toporov (DMT) model. Here two different regions are present, with the upper area having a higher stiffness compared to the bottom part. C) Another CON topographical area, with the adhesion map shown in D. Use of adhesion map facilitates the identification of SOM particles, with rounded and filamentous SOM components presenting adhesion values lower than the underlying mineral phase. E) A $9 \mu\text{m}^2$ APW area is displayed, which has been cleaned of most of the SOM component. F) Elastic Modulus E map of the area in E. This map reveals a homogeneous stiffness area, in contrast with the two stiffness components in B for a CON area. G) Another APW area, with the respective adhesive map shown in H. Few SOM remnants are left on the mineral surface (indicated by dark blue arrows). Colour Bars have a 0 baseline for all images.

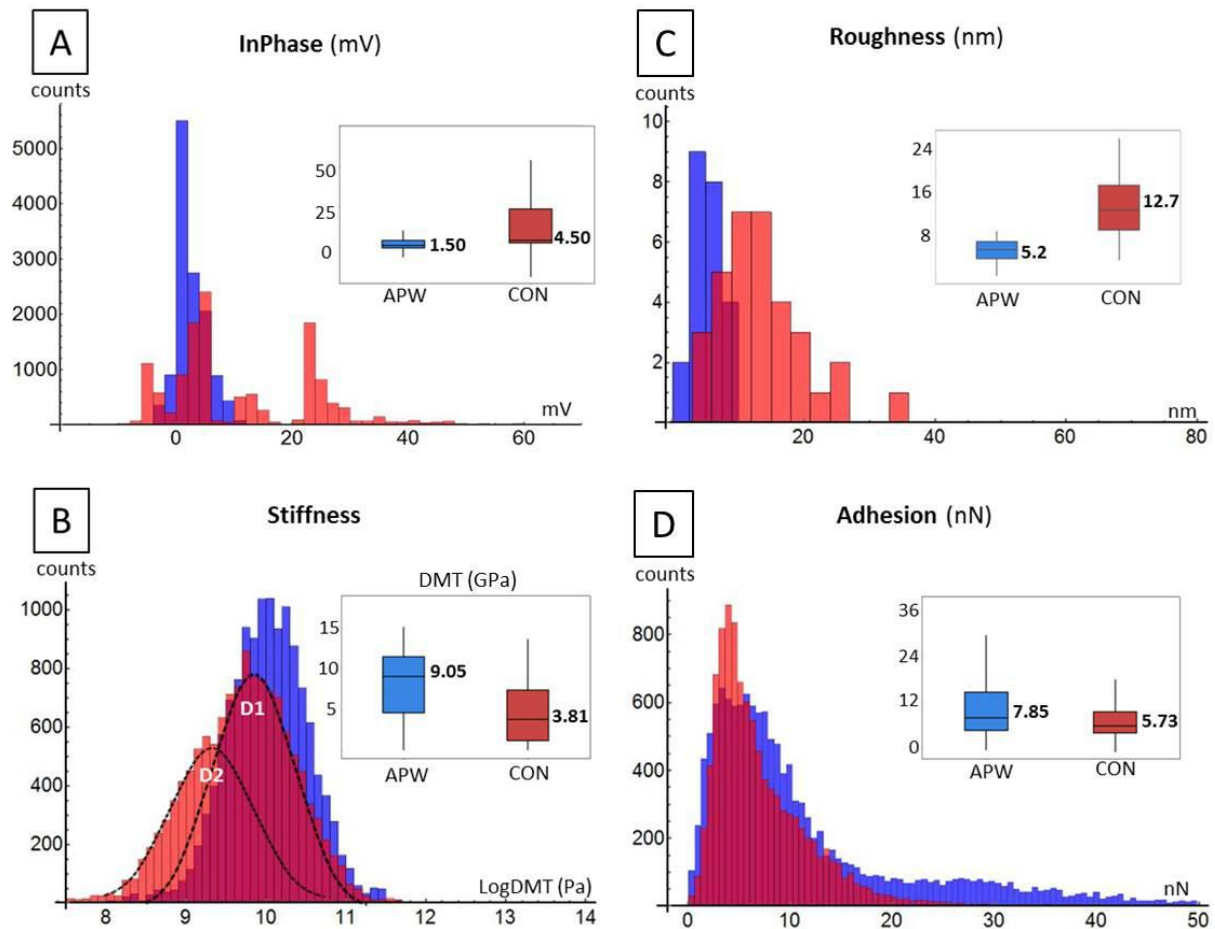


Figure 3. **Nanomechanical properties of organic and mineral components of soil aggregate surfaces.** Median values are expressed in boxplot graphs. A) InPhase histogram and boxplot for APW (blue) and CON (red) samples. Presence of organic matter in CON determines a scattering of values, indicating a higher variability in surface properties. B) Stiffness histogram (LogDMT) and boxplot (DMT) for CON and APW samples. Presence of organic matter in CON samples is indicated by a decrease in soil stiffness median value, 3.81 GPa, compared to APW samples, 9.05 GPa, where the stiff mineral phase is the main contributor to the measured AFM stiffness. While APW samples present a unique, Gaussian-like distribution, CON samples show two contributors, D1 and D2. C) Roughness calculated on APW and CON samples. Presence of organic matter in CON determines a greater roughness median and data distribution compared to APW sample. D) Adhesion histogram and boxplot for CON and APW samples. APW samples present a higher median value compared to CON samples, as indicated by the tail in data distribution in the histogram.

Table 1. Summary of data on APW and CON soil obtained with AFM, goniometry and Water Drop Penetration Test (WDPT).

	Parameter	APW Soil	CON Soil
AFM QNM	Stiffness (GPa)	9.05 ± 0.03	3.81 ± 0.03
	InPhase (mV)	1.50 ± 0.02	4.50 ± 0.12
	Roughness (nm)	5.2 ± 0.5	12.7 ± 1.2
	Organic Coverage (%)	8 ± 2	50 ± 7
	Adhesion (nN)	7.85 ± 0.10	5.73 ± 0.05
Other Techniques	Contact angle (Picolitre goniometry)	72.8° ± 3.1°	113.9° ± 2.9°
	Contact angle (Microlitre goniometry)	94.2° ± 4.3°	128.3° ± 6.1°
	WDPT (s)	5.3 ± 0.1	8815.2 ± 528.0

SUPPORTING INFORMATION

Organic matter identifies the nano-mechanical properties of native soil aggregates

Salvatore A. Gazze^{a*}, Ingrid Hallin^b, Gerry Quinn^c, Ed Dudley^a, Peter G. Matthews^b, Paul Rees^d, Geertje van Keulen G.^a, Stefan H. Doerr^e, Lewis W. Francis.^a

^a Swansea University Medical School , Singleton Campus, Swansea SA2 8PP, UK

^b Faculty of Science and Engineering, Plymouth University, Drake Circus, Plymouth PL4 8AA, UK

^c Ruđer Bošković Institute, Bijenička cesta 54, 10000, Zagreb, Croatia

^d College of Engineering, Swansea University, Bay Campus, Swansea, SA1 8EN, UK

^e Department of Geography, College of Science, Swansea University, Singleton Campus, Swansea SA2 8PP, UK

* e-mail: s.a.gazze@swansea.ac.uk

Supporting Figures

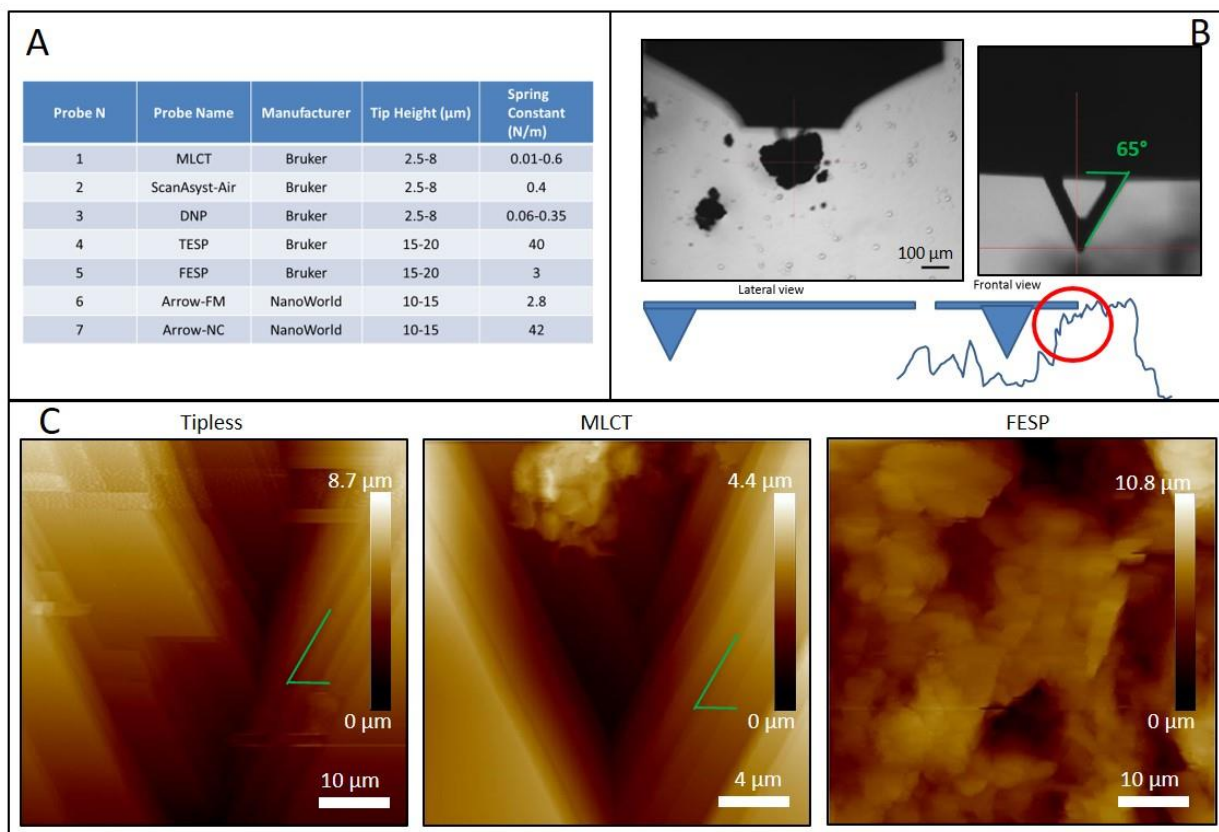


Figure S4. Performance of different cantilevers for soil aggregates. A) A list of the different probes tested, with manufacturers' values. The range of values reported for tip height is due to the inherent variability in manufacturing process, while the range of values for spring constant is due to the presence of several cantilever in the same chip having different spring constants. B) Clockwise from top-left corner, this panel represents: optical image of a cantilever positioned in the centre of a soil aggregate, which was previously immobilized on a thin layer of epoxy resin; detail of an MLCT cantilever, with the angle between the base and the cantilever; a schematic of the possible steric hindrance created by soil irregularities during cantilever scans. C) Scanning performance of different cantilevers (from left to right): a cantilever without tip produces images of terraces with the same angle reported in B; MLCT cantilevers often produce images similar to the ones of tipless cantilevers, demonstrating that the tip is unable to reach and scan the soil surface; cantilevers with longer tips are able to scan the soil surface in a more effective way and to produce images deprived of artefacts.

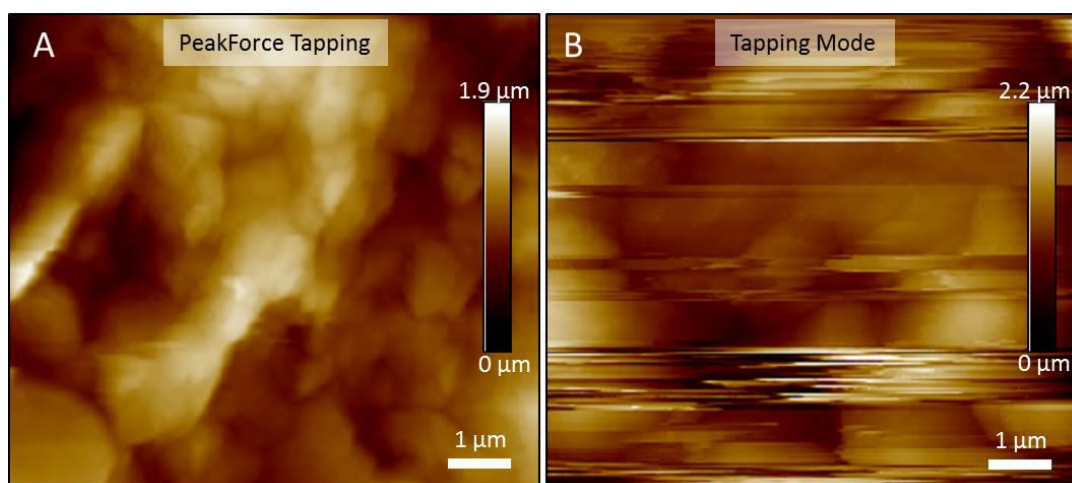


Figure S5. Performance of PeakForce Tapping (PFT) and Tapping Mode (TM) scanning. A) Peakforce Tapping is able to properly scan the soil surface, while Tapping Mode often produces streaks where the cantilever tip is unable to follow the irregular soil surface.

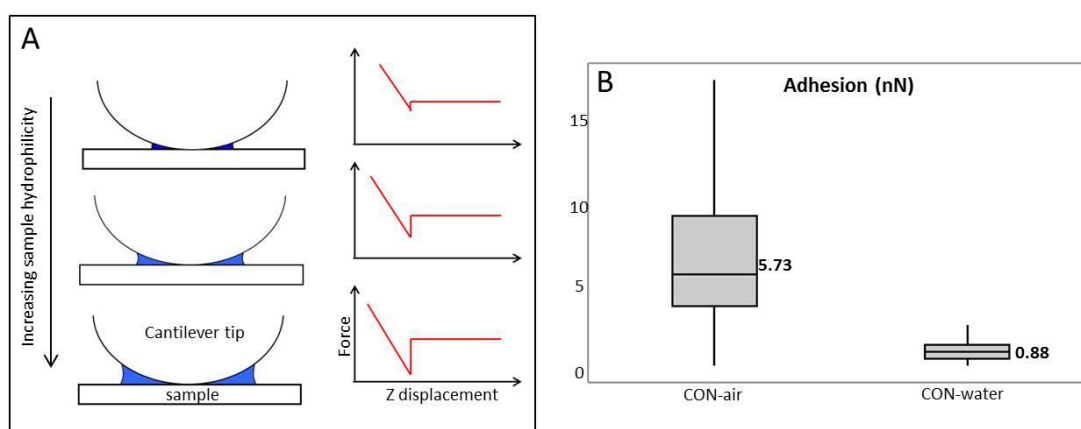


Figure S3. Surface hydrophilicity and adhesion pull-off force. A) In air an aqueous meniscus (blue in the schematic) forms between the cantilever tip and the scanned surfaces. Higher hydrophilicity increases the water meniscus and the associated pull-off force of the cantilever tip. B) Adhesion values measured on 30 soil CON areas in air (as already reported in Fig. 3D) and on 8 soil CON areas in water. The decrease in adhesion force in water is attributable to the absence of a meniscus force between the soil surface and the cantilever tip.

Supporting Tables

Coordinates	51°34'48"N 4°08'25"W
Particle Size Distribution	44.0 (±0.2)% sand 50.1 (±0.2)% silt 5.8 (±0.02)% clay
Texture	Silty loam
Organic matter (%)	5.60 ± 0.02
Total N (%)	0.210 ± 0.003
Total C (%)	3.20 ± 0.01
pH	6.27 ± 0.05
Bulk Density (g cm ⁻³)	1.18 ± 0.11

Table S1. Properties of Cefn Bryn soil used in this study.

Materials and Methods

Soil Collection, Characterization and Storage.

Soil was collected from under semi-natural grasslands at Cefn Bryn, Gower, Wales (51°34'48"N 4°08'25"W). A 5 x 5 m grid was laid out, five of the 25 squares were randomly selected (using a random number generator) for sampling, and within each of the 5 squares, a 50 cm square of turf was cut away on 3 sides and the soil from 5 to 10 cm depth was collected. Soil samples from all 5 squares were mixed in large plastic bags, sieved to 2 mm and thoroughly homogenised, and then stored at 4°C until testing. Soil characterization was conducted by Forest Research-Alice Holt Research Station (Surrey, UK). Particle size distribution was measured on pooled bulk soil using a Malvern Mastersizer 2000 (Worcestershire, UK) following organic matter removal by hydrogen peroxide flushing. Nitrogen and carbon was measured according to ISO methods 13878 and 10694, respectively, using a Thermo Scientific FlashEA® 1112 Nitrogen and Carbon Analyzer (Massachusetts, USA). Organic matter was measured using loss on ignition (LOI) technique. Soil pH was measured in water using a Spectrum Technologies Inc. IQ 150 pH meter (Illinois, USA). All soil physicochemical properties, reported in Table S1, are expressed as mean ± Standard Error of the Mean (SEM).

Acid-Peroxide Cleaning. Soil aggregates were cleaned from organic matter using the protocol reported in Mortlock and Froelich, 1989³². Briefly, 5 mL of 10% H₂O₂ is added to soil (between 25 to 200 mg) in a Falcon tube, and after 30 min, 5 mL of 1N HCl solution is added. The tube is then sonicated and left at room T for 30 min. 20 mL of deionized water is added and the tube is centrifuged at 4300 g for 5min. After supernatant removal, the soil sample is left to dry overnight at 60°C.

Goniometry and WDPT. Air dry, sieved (<2 mm) and homogenised soil samples were used for all goniometry and WDPT measurements, and all tests were carried out in ambient laboratory conditions (20-22°C and 35-50% RH).

For microlitre goniometry, three samples of each sample were prepared by filling small plastic weigh boats and levelling the surface. Three 80 µL drops of distilled water were deposited onto each sample, and high resolution videos were obtained using a KRÜSS DSA 25 (Hamburg, Germany). Contact angles for each drop were measured with the KRÜSS software using a linear baseline and a sessile drop (Laplace-Young) curve fit immediately following deposition. A single contact angle for each soil was determined by averaging the replicate contact angles and taking the standard deviation.

Picolitre goniometry samples were prepared by sprinkling the smallest grains of each soil across 4 small (approx. 1 mm²) squares of double-sided adhesive tape fixed to a microscope slide. The procedure was repeated three times to try to achieve a monolayer, and excess soil was removed by gently tapping the slide on its side after each application. HPLC grade water was dispensed onto the soil surface as 4 nL drops, and high resolution videos were obtained using a KRÜSS DSA 100M (Settings: 60V; 10,000 µs period; 100 µs pulse). Contact angles for each drop were calculated from screenshots of the drop immediately upon deposition using a linear baseline and a sessile drop (Laplace-Young) curve fit. A single contact angle for each soil was determined by averaging the replicate contact angles and taking the standard deviation.

The water drop penetration time (WDPT) of each soil sample type was determined by 30 x 80 µL drops of distilled water. A petri dish was filled with each soil and levelled before applying drops to the soil surface and noting the time from application to infiltration of each drop. A single WDPT was calculated for each soil by averaging all WDPT values. Data has been tested for normality using the Anderson-Darling test and a threshold p value of 0.05. All goniometry and WDPT values are expressed as mean (parametric data)/median (non-parametric data) ± Standard Error of the Mean (SEM).

Sample preparation for Atomic Force Microscopy (AFM). Soil samples were left to equilibrate at ambient conditions (T=21°C, RH≈ 50%) for 24 hours. Soil was gently sprinkled on an area of glass slide previously covered with a thin layer of a two-component epoxy, EPO-TEK 302-3M from Epoxy Technology Inc. (Billerica, U.S.A.), previously left to dry in air for about 6 hours in order to harden the glue enough to not engulf the soil aggregate particles. An optical microscope was used to check that the single aggregates only immobilized and were not engulfed in the epoxy glue. Samples were left to further dry in air for additional 24 hours before AFM analysis. An optical microscope was used to localize the aggregates for AFM scan and to position the cantilever tip above the soil aggregate.

AFM and Quantitative NanoMechanical Analysis (QNM). A Bruker BioScope Catalyst (Bruker Instruments, Santa Barbara, California, USA) was used to scan soil aggregates. MPP-21200-10 cantilevers (FESP, probe n.3 in Figure S1A, Bruker Instruments, Santa Barbara, California, USA) were used, with a nominal spring constant of 3 N/m, a nominal resonant frequency of 75 kHz and a silicon tip with a nominal height of 15-20 µm. The cantilever was calibrated on clean sapphire surface and spring constant and deflection sensitivity determined. All imaging was conducted using Peak Force

Tapping Mode (PF-TM) in Quantitative Nanomechanical Mode (QNM) at a scan speed of 1-0.5 Hz. Each image had a pixel resolution between 128x128 and 512x512, and one area per soil aggregate was scanned, with a total of about 30 areas per soil sample. A constant force of 5 nN was applied during scans. PFT-QNM calculated adhesion maps from the force required to detach the cantilever tip during the retraction cycle (“pull-off” force). Stiffness maps were reported as Derjaguin–Muller–Toporov (DMT) and LogDMT maps, where the modulus was obtained from the approach part of the force curves using the DMT model²¹. Nanoscope Analysis software, v1.50, was used to calculate roughness R_q using the equation:

$$R_q = \sqrt{\frac{\sum Z_i^2}{N}} \quad (1)$$

where, N is the number of points in the considered area and Z_i is the vertical displacement of each point i from the average data plane. Off-line analysis of topography images consisted of first order flattening and plane fitting. ImageJ® was used to calculate the areas occupied by organic matter. Raw data from QNM AFM outputs was extracted in ASCII format, plotted and analysed using Mathematica 10.0 and Minitab 17. Data has been tested for normality using the Anderson-Darling test and a threshold p value of 0.05. All AFM values are expressed as median \pm Standard Error of the Mean (SEM).